Mon. Not. R. Astron. Soc. **330,** 907–919 (2002)

# An Eulerian perturbation approach to large-scale structures: extending the adhesion approximation

N. Menci★
*Osservatorio Astronomico di Roma, via dell'Osservatorio, I-00040 Monteporzio, Italy*

Accepted 2001 November 6. Received 2001 November 5; in original form 2001 March 2

**ABSTRACT**

A description of the dynamics of a collisionless, self-gravitating fluid is developed and applied to follow the development of large-scale structures in the Universe. Such a description takes on one of the assumptions of the adhesion approximation (AA) model, i.e., the introduction of an artificial viscosity $\nu$ in the Euler equation, but extends it to deeper non-linear stages, where the extrapolation of the linear relation $\psi = -\phi$ between the velocity and the gravitational potentials – at the basis of both the Zel'dovich and the adhesion models – is no longer valid.

This is achieved by expanding the relation between $\phi$ and $\psi$, in general not explicitly computable, in powers of the small viscosity $\nu$. In this case, the evolution of the velocity potential is described by a diffusion-like equation for the 'expotential' field $\xi = \exp(-\psi/2\nu)$. Such an equation includes a source term $V(\xi)$, which expresses the relation between $\phi$ and $\psi$ as a series expansion in powers of $\nu$. Such a term is related to the onset of the non-linear evolution of the velocity potential and grows from zero (the limit corresponding to the AA) with increasing time. For terms in $V(\xi)$ up to order $O(\nu)$ (the only ones that can be expressed in a fully Eulerian form), the diffusion equation is solved using the path-integral approach.

The AA is then recovered as a 'free-particle' theory [corresponding to $V(\xi) = 0$], where the dynamics is determined by the initial value of $\xi$. Our inclusion of the lowest order term in $V(\xi)$ substantially changes the dynamics, so that the velocity potential at a given time in a given Eulerian position depends on the values taken at all previous times in all other coordinates. This is expected in the non-linear regime, where perturbations no longer evolve independently, but 'feel' the changes of the surrounding density field.

The path-integral solution is computed numerically through an algorithm based on Monte Carlo realizations of random walks in the Eulerian space. In particular, the solution $\xi$ at any cosmic time is obtained upon averaging the value of the potential $V(\xi)$ at previous times in the Eulerian locations reached by the random walks.

The solution is applied to the cosmological evolution of a cold dark matter density field, and the results are compared to the outcomes of an $N$-body simulation with the same initial condition. The velocity field in the presented extended adhesion (EA) description is obtained numerically using the random walks algorithm described above. For the case of a null potential $V(\xi) = 0$, this constitutes a novel implementation of the AA which is free from the numerical errors affecting finite-difference solution schemes for partial differential equation and is faster than the Gaussian convolution algorithm adopted by Weinberg & Gunn. When the first-order term of the potential $V(\xi)$ is included, the proposed extension of the adhesion approach provides a better description of small-scale, deeply non-linear regions, as is quantitatively shown by the computation of some statistical indicators. At larger scales, the satisfactory description of the large-scale texture and of the voids given by the canonical AA is preserved in the extended model.

**Key words:** hydrodynamics – galaxies: formation – cosmology: theory – large-scale structure of Universe.

★E-mail: menci@coma.mporzio.astro.it

## 1 INTRODUCTION

The formation of cosmic structures in the Universe is one of the key problems in cosmology. In the current, standard theory (see, e.g., Peebles 1993), they develop from the amplification of initially small density perturbations due to gravitational instability. For a collisionless self-gravitating fluid (similar to the non-baryonic dark matter, believed to dynamically dominate the Universe), the description of such a process is given by the usual hydrodynamical equations for the velocity and the density fields (Euler and continuity equations) in expanding coordinates, plus the Poisson equation coupling the gravitational potential $\phi$ to the density field $\delta$. In the linear stage, when the growing density is sufficiently small, such equations can be solved analytically using a first-order perturbation technique for the Eulerian density and velocity fields; higher order perturbation theory can give insights on the quasi-linear regime where, though small, $\delta$ becomes comparable to unity (see, e.g., Munshi, Sahni & Starobinsky 1994); however, the non-linear regime when $|\delta| > 1$ is usually followed in detail through numerical $N$-body simulations (see Bertschinger 1998 for a review). These show that gravitational instability of dark matter can indeed lead to the kind of large-scale structures observed in the Universe (starting from de Lapparent, Geller & Huchra 1986; see Maddox et al. 1990, Saunders et al. 1991, Vogeley et al. 1992 and Schectman et al. 1996), which include filamentary overdensities and two-dimensional sheet-like structures, the so-called pancakes; at the confluence of such one- or two-dimensional structures, high-contrast ($\delta > 200$), knotty structures appear to form, corresponding to galaxy clusters.

At the same time, several approximation schemes and semi-analytical approaches have been developed for studying the formation of large-scale structures (LSS). The aim of such approaches is to gain an insight into the physical processes leading to structure formation, to comprehend and check the results of the simulations, and to provide a computational tool which is usually faster and easier to implement.

The first step in an analytic approach to LSS was taken by Zel'dovich (1970), who proposed to extrapolate the linear behaviour of the velocity field to the non-linear regime and to express the evolution of each particle in terms of its Lagrangian coordinates. In this case, the trajectory of each particle evolves along the free-flight path determined by the initial Lagrangian velocity (for a review see, e.g., Shandarin & Zel'dovich 1989). In terms of the velocity potential $\psi$ (as long as no orbit-crossing occurs, the flow is irrotational and the velocity can be expressed as $\nabla\psi$), it can be easily shown that this corresponds to assume the velocity potential equal to the gravitational potential, a condition which holds in linear theory. The Zel'dovich approximation (ZA) turned out to work surprisingly well, even beyond the regime where its approximations are realistic (see, e.g., Melott et al. 1983, Shandarin & Zel'dovich 1989 and Sahni & Coles 1995). However, it presents some shortcomings, which can be traced back to the neglect of the back-reaction of the evolving density field on the gravitational field, and hence on the particle velocities. Thus, small-scale variations are transferred to much larger scales, resulting in a poor description of overdense regions; the collapse time of condensations is in general overestimated; the absence of a restoring force results in the formation of multistream regions, due to the crossing of particle orbits, so that pancakes thicken indefinitely after their formation.

To overcome the above problems, several improvements have been proposed. The Lagrangian perturbation theory developed by several authors (see Moutarde et al. 1991, Buchert & Ehlers 1993 and Bouchet et al. 1995) includes the ZA as a first-order solution; at higher orders, the particle displacement field is determined not only by the initial Lagrangian velocity (as in the ZA), but also by the acceleration field. When compared with $N$-body simulations (see Bouchet et al. 1995 and Melott, Buchert & Weiss 1995), the higher order Lagrangian approach turns out to improve the ZA for what concerns the first collapsing objects, the statistics of overdense regions and the compactness of clusters; on the other hand, underdense regions are better described in the ZA. In any case, the thickening of pancakes after shell-crossing remains a major drawback of such elaborate models.

Alternative approaches aiming at overcoming the thickening of pancakes typical of the ZA are constituted by the frozen-flow approximation (Matarrese et al. 1992), the linear potential approximation (Brainerd, Scherrer & Villumsen 1993; Bagla & Padmanabhan 1994) and the adhesion approximation (AA) (Gurbatov & Saichev 1984; Gurbatov, Saichev & Shandarin 1985, 1989; for reviews see Shandarin & Zel'dovich 1989, Vergassola et al. 1994 and Sahni & Coles 1995).

The first two propose to 'freeze' the initial velocity and potential field, respectively, to their initial value; particles then move with a velocity determined by the local Eulerian value of the initial velocity potential (or following the line of force of the initial gravitational potential in the linear-potential approximation). Such approaches avoid the shell-crossing occurring in the ZA but, as shown by comparison with aimed $N$-body simulations (Sathyaprakash et al. 1995), break down relatively early, soon after the non-linear length-scale exceeds the mean distance between peaks of the gravitational potential; in particular, the frozen-flow approximation, though reproducing reasonably well the density probability distribution of the dark matter field, fails in moving the mass particles to the right places when compared with the $N$-body simulations.

The AA, on the other hand, takes on the basic assumption of the ZA (i.e., the equality of the gravitational and velocity potentials) and introduces an artificial viscosity into the Euler equation to avoid orbit-crossing. Though introduced phenomenologically, later investigations by Buchert & Dominguez (1998) show that it is indeed possible to obtain viscosity-like terms from kinetic theory of self-gravitating collisionless systems (although the corresponding multistream forces are, in general, anisotropic, unlike the assumption of the AA). The effect of the viscosity $\nu$ in the limit $\nu \rightarrow 0$ can be straightforwardly computed; particles initially follow their linear trajectories (the same as in the ZA), but when flow lines intersect, the colliding particles stick to each other, thus binding collapsed structures and fixing the principal failure of the ZA. The networks of structures resulting from implementations of the AA have a remarkable resemblance to those emerging from $N$-body simulations; indeed, the rms density fluctuations agree to better than 20 per cent on scales larger than $\sim$5 Mpc (Weinberg & Gunn 1990a; Kofman et al. 1992; see also Melott, Shandarin & Weinberg 1994). Such agreement makes the AA a reliable tool for several astrophysical applications concerning LSS (see, e.g., Nusser & Dekel 1990 and Weinberg & Gunn 1990b).

Despite of the successes listed above in reproducing the texture of LSS, the AA model is a much less satisfactory description when structures at smaller scales are considered (Weinberg & Gunn 1990a; Kofman et al. 1992). The density field is less clumpy than appears in $N$-body simulations, where walls and filaments fragment into dense clumps, at variance with the outcomes of the AA. This is, of course, a consequence of

neglecting the back-reaction of the particle distribution on the evolution of the velocity field.

Here I propose an Eulerian approach to extend the AA to deeper, non-linear regimes. It allows me both to avoid the shell-crossing problem of the ZA and to go beyond the approximation (valid in the linear regime) stating the equality between the velocity and the gravitational potential, which is the basic Ansatz of both the ZA and AA descriptions. As a result, the velocity field felt by a particle at any given time is affected by the dynamical evolution occurring up to the considered time, as it must be in the non-linear regime (see Coles & Chiang 2000).

The equation governing the evolution of the *velocity field* is found by expanding the relation between $\phi$ and $\psi$, in general not explicitly computable, in powers of the small viscosity $\nu$. In this case, the Bernoulli equation, which governs the evolution of the velocity potential in the AA, can be recast [after the Hopf–Cole transformation $\xi = \exp(-\psi/2\nu)$] as a diffusion-like equation with a source term $V(\xi)$ constituted by an expansion in powers of $\nu$; such a term expresses the departure of the velocity field $\psi$ from the linear behaviour $\psi = -\phi$, assumed to hold in the AA. Since the lowest order term in $V(\xi)$ can be expressed in a completely Eulerian form, it is possible to solve such an equation in the Eulerian space *in this restricted case*.

The solution is obtained using the formalism of Brownian motion, equivalent to the path-integral formulation used in quantum mechanics and in statistical physics. In the limit of small times, $V(\xi) \rightarrow 0$ (corresponding to a null potential in the language of path-integrals), one recovers the standard AA, which thus constitutes, in the language of path-integrals, a free-particle theory (see also Jones 1999) whose solution is determined in terms of the initial field; the first-order term of the potential $V(\xi)$ – corresponding to a 'theory with interactions' in the language of path-integrals – introduces the non-linear corrections to the AA; the solution at a generic time depends not only on the initial field, but also on its values at all previous times and at all other coordinates.

To test the proposed description, the solution is applied to the cosmological evolution of a cold dark matter density field. The corresponding velocity field is obtained numerically at any time by constructing – for each Eulerian coordinate – a set of random trees, which are used to compute the path-integrals with specific forms of the interaction potential. For a null potential, this constitutes a novel implementation of the AA which is free from the numerical errors affecting finite-difference solution schemes for partial differential equation, and is faster than the Gaussian convolution algorithm adopted by Weinberg & Gunn (1990a); when the first-order term in the path-integral potential is included, the evolved field gives a better description of small-scale, deeply non-linear regions, as shown by the comparison with an appropriate *N*-body simulation.

The plan of the paper is as follows. The Bernoulli equation for the velocity potential $\psi$ typical of the AA model is introduced and extended beyond the linear evolution (Section 2). After a canonical change of variables (the Hopf–Cole transformation), such an equation is transformed into a diffusion-like equation for $\xi$ with a potential term which expresses the non-linear evolution of the transformed velocity potential. The latter term is expanded in powers of the artificial viscosity; the solution for the leading order is obtained using the path-integral formalism (Section 3), and it is numerically implemented through the construction of random walks for the transformed velocity field (Section 4). The results (Section 5) are then compared with the outputs of an *N*-body simulation with a cold dark matter power spectrum for the initial density perturbation field. Sections 6 and 7 are devoted to conclusions and discussion.

## 2 BASIC DYNAMICS

It can be easily shown that the Euler equation for a collisionless self-gravitating fluid in the Newtonian limit in the expanding Universe can be conveniently rewritten as a Bernoulli equation for the velocity potential, when rescaled variables are used (Gurbatov et al. 1989; Kofman 1991). If the comoving peculiar velocity field $\boldsymbol{u} = \nabla\psi\dot{a}$ is expressed in terms of the gradient of a velocity potential $\psi$ and of the time derivative of the expansion factor $a$, then the evolution of the velocity potential is governed by

$$\frac{\partial\psi}{\partial a} + \frac{1}{2}(\nabla\psi)^2 = -\frac{3}{2a}(\phi + \psi). \tag{1}$$

Here $\phi$ is the gravitational potential divided by $3t_0^2/2a_0^3$, where $t_0$ and $a_0$ are the initial time and expansion factors, respectively.[1]

The ZA can be recovered from equation (1) imposing that $\phi = -\psi$, a condition which is valid in the linear regime. The solution of equation (1) is then

$$\psi(\boldsymbol{x}, a) = \psi_0(\boldsymbol{q}) + \frac{(\boldsymbol{x} - \boldsymbol{q})^2}{2(a - a_0)}, \tag{2}$$

where $\boldsymbol{x}$ and $\boldsymbol{q}$ are the Eulerian and Lagrangian coordinates of a particle with trajectory $\boldsymbol{x}(\boldsymbol{q}, a)$. The solution of equation (1) is characterized by the remarkable property that $\nabla_{\boldsymbol{x}}\psi(\boldsymbol{x}, a) = \nabla_{\boldsymbol{q}}\psi_0(\boldsymbol{q})$. Thus the particles trajectories are flee-flights with $\boldsymbol{x} = \boldsymbol{q} + (a - a_0)\boldsymbol{u}_{\boldsymbol{q}}$ determined by the initial velocity $\boldsymbol{u}_{\boldsymbol{q}} = \nabla\psi_{\boldsymbol{q}} = -\nabla\phi_{\boldsymbol{q}}$.

The AA consists in keeping the Ansatz $\phi = -\psi$, but adding to the left-hand side of equation (1) a viscosity term $-\nu\nabla^2\psi$. With the Hopf–Cole transformation $\psi = -2\nu\ln\xi$, the Bernoulli equation (1) is transformed into a linear diffusion equation $\partial\xi/\partial a = \nu\nabla^2\xi$, where the expansion factor plays the role of time; the solution is well known to be the convolution of the initial condition with a Gaussian whose variance is proportional to the time variable. Transforming back the solution for $\xi$ into the velocity potential, one obtains the expression for $\psi$ in the AA, which reads

$$\psi(\boldsymbol{x}, a) = -2\nu\ln\left[\frac{1}{4\pi\nu(a - a_0)^{3/2}}\int \mathrm{d}^3q\, \mathrm{e}^{-\frac{1}{2\nu}S(\boldsymbol{x},\boldsymbol{q},a)}\right], \tag{3}$$

where the action is

$$S(\boldsymbol{x}, \boldsymbol{q}, a) = \psi_0(\boldsymbol{q}) + \frac{(\boldsymbol{x} - \boldsymbol{q})^2}{2(a - a_0)}. \tag{4}$$

It can be shown (see, e.g., Vergassola et al. 1994) that, in the limit $\nu \rightarrow 0$, the solution reads

$$a\psi(\boldsymbol{x}, a) = \sup_{\boldsymbol{q}}\left[a\psi_0(\boldsymbol{q}) - q^2/2 + \boldsymbol{x}\cdot\boldsymbol{q}\right] - x^2/2. \tag{5}$$

The confluence of different Lagrangian points into a single Eulerian coordinate gives rise to the formation of caustics and knots, reproducing the skeleton of LSS, and avoiding the shell-crossing. Indeed, given a coordinate $\boldsymbol{x}$ at a time corresponding to $a$, the Lagrangian points corresponding to orbits leading to $\boldsymbol{x}$ are all

[1] Whenever irrelevant for the exposition and for the computations, the spatial argument $\boldsymbol{x}$ will be omitted; the dependence on the expansion factor will be often indicated with a subscript, so that $\psi(\boldsymbol{x}, a)$ will be often indicated as $\psi_a$. The subscript 0 will be used for fields computed at the initial time, so that $\psi_0 \equiv \psi_{a_0}$.

the $\boldsymbol{q}_*$ where the maximum in equation (5) is attained. Shell-crossing does not occur in the AA, since the property that $[\boldsymbol{q}_*(\boldsymbol{x},t)-\boldsymbol{q}_*(\boldsymbol{x}',t)]\cdot(\boldsymbol{x}-\boldsymbol{x}')\geq 0$ holds.

## 3 EXTENDING THE ADHESION APPROXIMATION

All the schemes discussed above are characterized by the extrapolation of the relation $\psi=-\phi$ to the non-linear regimes, with the resulting limitations discussed in the Introduction.

A step forward can be made considering the remaining equations for the dark matter fluid. The continuity equation can be recast in terms of the rescaled density field $\eta=\delta+1$ to read

$$\frac{\partial\eta}{\partial a}+\boldsymbol{u}\cdot\nabla\eta+\eta\nabla\cdot\boldsymbol{u}=0. \tag{6}$$

A formal solution of the above equation can be found upon integrating along the particle trajectory $\boldsymbol{x}(a)$, where $\boldsymbol{x}$ is the comoving Eulerian coordinate. Then one obtains

$$\delta(\boldsymbol{x},a)=[\delta_0(\boldsymbol{q})+1]\,\mathrm{e}^{-\int_{\mathcal{C}_a(x)}\mathrm{d}a'\nabla\cdot\boldsymbol{u}[\boldsymbol{x}(\boldsymbol{q},a'),a']}-1, \tag{7}$$

where integration over $\mathcal{C}_a(x)$ indicates integration over the particle trajectory from the Lagrangian coordinate $\boldsymbol{q}$ at the initial time $a_0$ to the Eulerian position $\boldsymbol{x}$ at the time corresponding to $a$. The above density field is related to the gravitational potential by the Poisson equation

$$\nabla^2\phi=\frac{\delta}{a}. \tag{8}$$

To obtain an equation for $\psi$, we start from equation (1) modified with the addition of the viscosity term $-\nu\nabla^2\psi$ on the left-hand side After substituting to $\nabla^2\phi$ the value $\delta(x,a)/a$ obtained from equation (8), one finally obtains

$$\frac{\partial\Delta\psi}{\partial a}+\frac{1}{2}\Delta(\nabla\psi)^2-\nu\Delta\nabla^2\psi = -\frac{3}{2a}\left\{\frac{(\delta_0(\boldsymbol{q})+1)\,\mathrm{e}^{-\int_{\mathcal{C}_a(x)}\mathrm{d}a'\Delta\psi[\boldsymbol{x}(\boldsymbol{q},a'),a']}-1}{a}+\Delta\psi\right\}. \tag{9}$$

To transform the left-hand side of equation (9) into a diffusion term, we perform the canonical Hopf–Cole transformation $\psi=-2\nu\ln\xi$, to obtain

$$\Delta\left(-\frac{2\nu}{\xi}\frac{\partial\xi}{\partial a}+\frac{2\nu^2}{\xi}\Delta\xi\right) = -\frac{3}{2a}\left\{\frac{[1+2a\nu\Delta\ln\xi_0(\boldsymbol{q})]\,\mathrm{e}^{2\nu\int_{\mathcal{C}_a(x)}\Delta\ln\xi\,\mathrm{d}a'}-1}{a}-2\nu\Delta\ln\xi\right\}, \tag{10}$$

where we have used the property that $\delta_0(\boldsymbol{q})=-a\Delta\psi_0(\boldsymbol{q})=2\nu a\Delta\ln\xi_0(\boldsymbol{q})$, valid in the linear regime, as appropriate, since the above quantities are computed at the initial time corresponding to $a_0$.

We seek for a perturbation expansion of the right-hand side of the above equation, which at lowest order must be zero (according to linear theory and to the Ansatz in the ZA and the AA) and at higher orders detach from the null value according to the growth of structures in the non-linear regime. To this aim, we expand the exponential on the right-hand side in powers of the small viscosity $\nu$. Keeping terms up to $O(\nu^2)$ (the order of the diffusion term on the left-hand side), one obtains

$$\frac{\partial\xi}{\partial a}-\nu\Delta\xi=\frac{3}{2a}\xi V(\xi), \tag{11a}$$

$$V(\xi)\equiv\Delta^{-1}\left[\frac{a\Delta\ln\xi_0(\boldsymbol{q})+\int_{\mathcal{C}_a(x)}\Delta\ln\xi\,\mathrm{d}a'+(\nu/2)\left(\int_{\mathcal{C}_a(x)}\Delta\ln\xi\,\mathrm{d}a'\right)^2}{a} +2\nu\Delta\ln\xi_0(\boldsymbol{q})\int_{\mathcal{C}_a(x)}\Delta\ln\xi\,\mathrm{d}a'-\Delta\ln\xi\right]. \tag{11b}$$

The computation of all terms involving the inverse-Laplacian operator $\Delta^{-1}$ is, of course, extremely difficult. It is possible, however, to *put in evidence* some of the terms in the 'potential' $V(\xi)$. In particular, it turns out (see Appendix A) that

$$\Delta^{-1}Q_a\equiv\Delta^{-1}\left[\int_{\mathcal{C}_a(x)}\Delta\ln\xi\,\mathrm{d}a'\right] =\int_{a_0}^{a}\mathrm{d}a'\ln\xi_{a'}+2\nu\Delta^{-1}\int\nabla Q\cdot\nabla\ln\xi_{a'}\,\mathrm{d}a' \tag{12}$$

and

$$\Delta\ln\xi_0(\boldsymbol{q})=\Delta\ln\xi+2\nu\int_{\mathcal{C}_a(x)}\nabla(\Delta\ln\xi)\cdot\nabla\ln\xi\,\mathrm{d}a'. \tag{13}$$

Inserting the above equations into equations (11a) and (11b), these can be written in compact form as a diffusion equation with a source term (or Shrödinger-like equation in Euclidean time):

$$\frac{\partial\xi}{\partial a}=\nu\Delta\xi+\frac{3}{2a}\xi(V_1+\nu V_2), \tag{14a}$$

$$V_1=\int_{a_0}^{a}\ln\xi_{a'}\,\mathrm{d}a'/a\equiv\overline{\ln\xi_a}, \tag{14b}$$

$$V_2=\Delta^{-1}\left[\frac{2\int\nabla Q\cdot\nabla\ln\xi_{a'}\,\mathrm{d}a'}{a}+\frac{(\int_{\mathcal{C}_a(x)}\Delta\ln\xi\,\mathrm{d}a')^2}{2a} +\frac{2\Delta\ln\xi_0(\boldsymbol{q})\int_{\mathcal{C}_a(x)}\Delta\ln\xi\,\mathrm{d}a'}{a}+2\int_{\mathcal{C}_a(x)}\nabla(\Delta\ln\xi)\cdot\nabla\ln\xi\,\mathrm{d}a'\right]. \tag{14c}$$

The above equation shows that the non-linear dynamics with viscosity is modified with respect to the AA by the effect of two terms. (i) A sort of 'time-average' of the velocity field, corresponding to 'potential' $V_1$; this constitutes the lowest order modification to the linear Ansatz $\psi=-\phi$ of AA. (ii) An explicitly non-local term $V_2$, involving the inverse Laplacian; of course, it is overwhelmingly difficult to compute any of the terms contained in $V_2$.

In the following, the solution of equation (14) will be restricted to the first term $V_1$, the one that is treatable in a fully Eulerian form; we shall refer to the corresponding dynamics as the extended adhesion (EA) model. Note that the other term $V_2$ enters the equations multiplied by the small viscosity $\nu$, so that its effects on the dynamics should be small. Although this is an encouraging property, a rigorous full perturbative solution of equation (14) would require keeping the terms up to order $\nu$, since this is the order of the diffusive term $\nu\Delta\xi$ characteristic of adhesion models.

The lowest order (in $\nu$) term of the potential (the 'time-average' in $V_1$) is expected to introduce relevant modifications to the dynamics with respect to the AA, thus representing a significant step forward in the description of the non-linear regime. First, we

note that the source term $V_1$ is growing from zero with increasing time ($V_1 \to 0$ for $a \to a_0$) as is expected for a term connected with the departure from linearity. Thus, for small times the system behaves much like the AA; at later times the term $V_1$ will set in, affecting the dynamics in the deeper non-linear regime. The first modification introduced by $V_1$ is that the velocity field at a given time is no longer determined by the initial field $\xi_0$, as was resulting from the linear Ansatz $\psi = -\phi$ characteristic of the ZA and the AA (see equations 2–4).

At early times, in the quasi-linear regime, further insight into the potential term $V_1$ can be gained by a series expansion of the velocity potential $\psi = \psi^{(1)} + \psi^{(2)}$ around the initial time $a_0$; terms of increasing order correspond to consider increasing powers of $a$. The dynamics resulting from equations (14a) and (14b) can be compared to the exact perturbation theory (valid for small density contrasts and close to the initial time) up to second order in $\psi$ (where exact solutions are available). The first-order term (the linear solution) is the same for the exact theory, AA and EA, namely $\psi^{(1)}(x) = -\phi_0(x)$; the second-order term in AA and EA can be obtained by inserting the first-order solution in the $(\nabla\psi)^2$ term in the Bernoulli equation 1 (at early times particles sticking occurring in AA and EA is unimportant, so that the viscosity term can be neglected in this restricted context) and letting $\psi = -\phi$ (for the AA, according to the Zel'dovich approximation) or $\phi + \psi = -\bar{\psi}$ for the EA (after transforming equations 14a and 14b back into the $\psi$ variable), where $\bar{\psi}$ is the average over $a$ of the velocity potential which we express as $\bar{\psi} \approx \beta\psi$. After the above procedure, the AA and EA solutions at second order are $\psi^{(2)}_{\rm AA} = -(1/2)\times(\nabla\phi_0)^2 a$ and $\psi^{(2)}_{\rm EA} = -[\beta/(3-2\beta)](\nabla\phi_0)^2 a$; these have to be compared with the exact second-order solution which contains a non-local term, i.e., $3/7\Delta^{-1}[\nabla(\nabla\phi_0\Delta\phi_0)]$, which is not reproduced by the AA or by EA with the potential $V_1$, plus a local term $\psi^{(2)}_{\rm exact} = -(6/21)(\nabla\phi_0)^2 a$ (see Munshi & Starobinsky 1994). Note that (for $\beta \approx 1/2$ at second order) the EA at second order yields $\psi^{(2)}_{\rm EA} = -(1/4)(\nabla\phi_0)^2 a$, which is closer to the exact term than the AA. Thus, when a time expansion of the velocity potential is considered for small times, the potential obtained from both the EA and AA have the same spatial structure as the local part of the exact second-order correction, but the EA is closer in normalization to the exact solution.

At later times, a property of the dynamics described by equations (14) is that the changes of the velocity field in the course of the evolution now explicitly affect the dynamics. In addition, as will be discussed in detail in Section 4.3, the presence of a potential $V(\xi)$ depending on $\xi$ in equation (14) introduces non-local features in the solution, so that the field $\xi(\boldsymbol{x}, a)$ depends on the value of the field at other Eulerian points. This feature is expected to arise in the non-linear regime, since the density fluctuations cease to evolve independently and 'feel' the effect of the whole mass distribution (we refer to Section 7 for a more extended discussion on the effects of the term $V_1$ on the overall evolution of LSS).

To quantitatively explore the above effects, we now proceed to solve the diffusion equation (14), restricting the consideration to only the first term $V_1$.

## 4 SOLVING THE DIFFUSION EQUATION: THE RANDOM WALK APPROACH

To discuss the solution of the diffusion equation (14) let us start with the simple case when no source term is introduced ($V_1 = V_2 = 0$ in equation 14); this corresponds to the AA. The approach used for this case will be then extended to include the term $V_1(\xi)$.

### 4.1 Free-diffusion: recovering the adhesion approximation

It is well known that the linear diffusion equation $\partial\xi/\partial a - \nu\Delta\xi = 0$ describes the time evolution of the probability distribution for a Gaussian random walk. Let us define a random variable $\boldsymbol{b}_s$ which, as time is incremented by a step d$s$, increments its value by a random amount $\delta\boldsymbol{b}$ extracted from a Gaussian distribution with variance $\sigma^2 = 2\nu\,\mathrm{d}s$ along a path whose time coordinate $s$ ranges from $a_0$ to the time $a$. Then the solution of equation (14) at the point $\boldsymbol{x}$ can be written in terms of the initial field $\xi_0$ computed at the locations $\boldsymbol{b}(a)$, i.e., the coordinate reached by the random path by the time $a$. In particular, the solution writes (see, e.g., Gärtner &

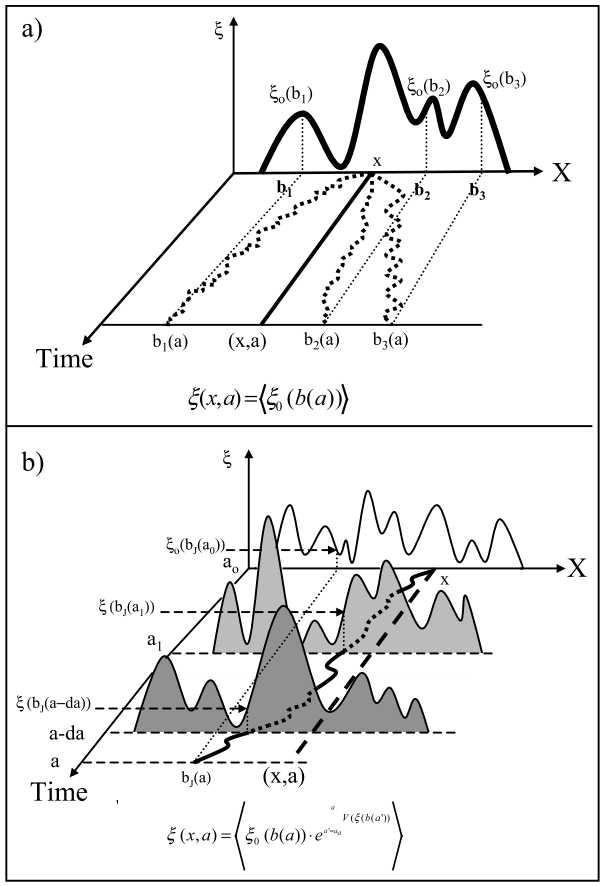


**Figure 1.** Panel (a): An illustration of the random-walk solution to the diffusion equation with no source term; for the sake of simplicity, the illustration is restricted to a one-dimensional space (indicated as $X$ in the label on the horizontal axis). To obtain the solution at the point $\boldsymbol{x}$ at time $a$, different realizations of a Gaussian random walk are constructed, with the condition that they all start from the Eulerian point $\boldsymbol{x}$ at time $a_0$; in the figure, three such paths are schematically illustrated and labelled $b_1(a)$, $b_2(a)$ and $b_3(a)$. The points $b_J(a)$ reached by the random walk at time $a$ are then projected backwards to the initial time $a_0$ (and labelled $b_1$, $b_2$ and $b_3$ in the picture). The average of the corresponding values of the *initial* field $\xi_0$ at such points [indicated as $\xi_0(b_1), \ldots, \xi_0(b_3)$] yields the solution. Panel (b): The corresponding graphical representation of the solution when a source term (of the kind of $V_1$ in equation (14) is introduced in the diffusion equation. Here, for the sake of simplicity, only one realization [indicated by $b_J(a)$] of the random walk is shown. To obtain the solution at time $a$, besides computing the initial field at the location $b(a)$ as in panel (a), all the field $\xi_{a'}$ at times $a' < a$ are required, and have to be computed at the points reached by the random walk at the times $a'$. Such values of the fields are used to compute the potential $V_1$; see point (iii) in the text. Again the solution is found upon averaging over all the realizations of the random walk.

Molchanov 1991)

$$\xi(\boldsymbol{x}, a) = \langle \xi_0[\boldsymbol{b}(a)] \rangle, \tag{15}$$

where the average refers to the ensemble of paths $\boldsymbol{b}_s$ departing from $\boldsymbol{x}$ at time 0. We indicate with $\boldsymbol{b}(a)$ the value of the random walk at time $a$.

Fig. 1(a) illustrates how this solution works, for the one-dimensional case where a simple visualization is possible. To find the function $\xi(\boldsymbol{x}, a)$, a number of realizations of the random walk are started from the point $\boldsymbol{x}$ at $a_0$. At the time $a$, each Eulerian point reached by the $J$th realization $\boldsymbol{b}_J(a)$ of the random walk is 'projected' at the initial time $a_0$ (the points $\boldsymbol{b}_1, \ldots, \boldsymbol{b}_n$ in Fig. 1a), and there the *initial* function $\xi_0(\boldsymbol{b}_J)$ is computed. The solution is obtained after averaging over all the possible $\boldsymbol{b}_J$, weighting by their probability to occur. Since for a Gaussian random walk this is a Gaussian with variance $\sigma^2(a) = 2\nu(a - a_0)$, the projections on the $a_0$ axis of the points $\boldsymbol{b}_J(a)$ (i.e., the points $\boldsymbol{b}_1, \ldots, \boldsymbol{b}_n$ in Fig. 1a) will deviate from the initial position $\boldsymbol{x}$ of the random walk with a probability

$$P(\boldsymbol{b}) = \frac{1}{[4\pi\nu(a - a_0)^{3/2}]} \mathrm{e}^{-\frac{1}{2\nu}(\boldsymbol{x}-\boldsymbol{b})^2/2(a-a_0)}. \tag{16}$$

According to what was said above, the solution at time $a$ is then

$$\xi(\boldsymbol{x}, a) = \int \mathrm{d}^3 b P(\boldsymbol{b}) \xi_0(\boldsymbol{b}). \tag{17}$$

Indeed, performing the Hopf–Cole transformation back to the velocity potential $\psi = -2\nu \ln \xi$, the velocity potential of the AA (equations 3 and 4) is obtained.

Note that the above solution can be written in the language of path-integrals, widely used in quantum mechanics (Feynman & Hibbs 1965):

$$\xi(\boldsymbol{x}, a) = \int K(\boldsymbol{x}, a, \boldsymbol{x}_0, a_0) \xi(\boldsymbol{x}, a_0)\, \mathrm{d}(\boldsymbol{x}_0). \tag{18}$$

The kernel $K$ is the particle propagator which is generally written as

$$K(\boldsymbol{x}, a, \boldsymbol{x}_0, a_0) = \int_{\boldsymbol{x}_0}^{\boldsymbol{x}} \mathrm{e}^{S[b(s)]} \mathcal{D}[b(s)]. \tag{19}$$

The integral on the right-hand side is actually a sum over all the random paths $b(s)$ that connect $\boldsymbol{x}_0$ at the initial time to $\boldsymbol{x}$ at the present time, the variable $s$ corresponding to the time variable of the random walk. The symbol $\mathcal{D}[b(s)]$ implies integration over positions at intermediate times in the random walk; for a discrete walk constituted by $n$-steps labelled $s_1, \ldots, s_n$, it takes the form $\mathcal{D}[b(s_n)] = \Pi_{i=0}^{n} b_{s_i}/\sqrt{4\pi(s_{i+1} - s_i)}$. The action $Sb(s)]$ actually weights the paths contributing to the integral. For the free diffusion equation the action is that of a free particle, containing only the 'kinetic' term $S = -\int (1/4\nu)[\mathrm{d}\boldsymbol{b}(s)/\mathrm{d}s]^2\, \mathrm{d}s$. Thus, in this language the AA (leading to a free-diffusion equation for the transformed velocity field $\xi$) corresponds to a free-particle theory.

### 4.2 Diffusion with a source term

The solution for a diffusion equation with a source term can be obtained generalizing the action in equation (19) to include the presence of a potential term. When $V(\xi)$ is included, the action takes the form

$$S(\boldsymbol{b}, a) = -\int_{a_0}^{a} \left\{ \frac{1}{4\nu} \left[ \frac{\mathrm{d}\boldsymbol{b}(s)}{\mathrm{d}s} \right]^2 - V[\xi(\boldsymbol{b}, s)] \right\} \mathrm{d}s. \tag{20}$$

When inserted into the path-integral (equations 18 and 19), this provides a solution to equation (14). Thus the terms $V_1$ in equation (14b) constitute an interaction potential proportional to the time average of the $\psi$. The non-linear effects in the evolution of the velocity field of a self-gravitating fluid with artificial viscosity are then mapped into a theory with interaction for the field $\xi$.

The random-walk representation of the solution defined by equation (20) is the analogue of equation (15), and reads (see Gärtner & Molchanov 1991)

$$\xi(\boldsymbol{x}, a) = \langle \xi_0(\boldsymbol{b}_a)\, \mathrm{e}^{\int_{a_0}^{a} V\{\xi[b(s)]\}\, \mathrm{d}s} \rangle. \tag{21}$$

Of course, since the function $\xi$ itself appears as an argument of the potential on the right-hand side, equation (21) actually represents an *equation* for $\xi$, which is equivalent to equation (14). To show such equivalence and to discuss how the above solution works, let us write the time evolution of the field $\xi(\boldsymbol{x}, a)$ satisfying equation (21):

$$\xi(\boldsymbol{x}, a + \mathrm{d}a) = \langle \xi_0[\boldsymbol{b}(a + \mathrm{d}a)] \mathrm{e}^{\int_{a_0}^{a+\mathrm{d}a} V\{\xi[b(s)]\}\, \mathrm{d}s} \rangle. \tag{22}$$

Expanding both the first and second factors in the average on the right-hand side, one obtains

$$\xi_0[\boldsymbol{b}(a + \mathrm{d}a)] = \xi_0[\boldsymbol{b}(a)] + \delta\boldsymbol{b} \cdot \nabla \xi_0[b(a)] + \tfrac{1}{2}(\delta\boldsymbol{b})^2 \nabla^2 \xi_0[\boldsymbol{b}(a)], \tag{23a}$$

$$\mathrm{e}^{\int_{a_0}^{a+\mathrm{d}a} V\{\xi[b(s)]\}\, \mathrm{d}s} = \mathrm{e}^{\int_{a_0}^{a} V\{\xi[b(s)]\}\, \mathrm{d}s} [1 + V\{\xi[b(s)]\}\, \mathrm{d}s]. \tag{23b}$$

We insert the above expansions into equation (22) and perform the average over the distribution function $p(\delta\boldsymbol{b})$. If this is symmetric and with variance $2\nu\, \mathrm{d}a$ (we choose it to be a Gaussian), then the terms proportional to $\delta\boldsymbol{b}$ cancel out, and we are left with

$$\xi(\boldsymbol{x}, a + \mathrm{d}a) = \langle \xi_0[\boldsymbol{b}(a)\, \mathrm{e}^{\int_{a_0}^{a} V\{\xi[b(s)]\}\, \mathrm{d}s} \rangle + \langle \xi_0[\boldsymbol{b}(a)]\, \mathrm{e}^{\int_{a_0}^{a} V\{\xi[b(s)]\}\, \mathrm{d}s} \rangle V(\xi(a)\, \mathrm{d}a + \nu\, \mathrm{d}a \nabla^2 \langle \xi_0[\boldsymbol{b}(a)]\, \mathrm{e}^{\int_{a_0}^{a} V\{\xi[b(s)]\}\, \mathrm{d}s} \rangle \tag{24}$$

out to order $O(\mathrm{d}a^2)$. Substituting equation (21) for the ensemble averages, dividing by $\mathrm{d}a$ and taking the limit $\mathrm{d}a \to 0$ yields equation (14) for a generic potential $V(\xi)$ on the right-hand side. This shows that equation (21) is a reformulation of equation (14) in terms of random walks.

### 4.3 Implementing the solution of the diffusion equation with source term

Here we shall take advantage of the formulation (21) to develop a numerical method for computing the solution of equation (14). This will allow to avoid the use of finite-difference schemes for integro-differential equations which are characterized by delicate numerical instabilities.

To solve equation (21) with numerical realizations of random walks, we first set up a grid of three-dimensional coordinates $\boldsymbol{x}$ and of time-steps, where the transformed velocity potential $\xi$ has to be computed. Then we proceed through the following steps.

(i) At the initial time $a_0$, for each Eulerian position $\boldsymbol{x}$, we assign the initial velocity field, and hence the initial field $\xi_0(\boldsymbol{x}) = \xi(\boldsymbol{x}, 0)$. We initialize $N_{\mathrm{real}}$ realizations of random walks, associated with

the considered Eulerian coordinate $\boldsymbol{x}$ with the initial condition $b_J^{\boldsymbol{x}}(a_0) = \boldsymbol{x}$, where $J$ is the label of the realization, $J = 1, \ldots, N_{\rm real}$. The initial value of the potential $V_1(\xi_0, a_0)$ in equation (14) is set equal to zero.

(ii) We increment the time-step by d$a$. For each coordinate $\boldsymbol{x}$ we update the random walk $b_J^{\boldsymbol{x}}(a)$ associated with it by extracting the increments $\delta \boldsymbol{b}_J$ from a Gaussian distribution (with variance $2\,\nu\,{\rm d}a$) for each realization $J$. For each coordinate $\boldsymbol{x}$, we update the variable $b_J^{\boldsymbol{x}}(a) = b_J^{\boldsymbol{x}}(a - {\rm d}a) + \delta_J \boldsymbol{b}$ for each realization $J$ of the random walk.

(iii) We compute $\boldsymbol{\xi}_0[b_J^{\boldsymbol{x}}(a)]$ by interpolating the initial field $\boldsymbol{\xi}_0$ in the point $b_J^{\boldsymbol{x}}(a)$.

We evaluate the action $S_J^{\boldsymbol{x}}(a) = S_J^{\boldsymbol{x}}(a - {\rm d}a) + V_1\{\xi_{a-da}[b_J^{\boldsymbol{x}}(a - {\rm d}a)]\}\,{\rm d}a$, entering the solution (21) using the value of the field $\xi$ at the previous time-step to compute the potential $V_1(\xi)$.

(iv) We compute numerically the average defining the solution equation (21) by summing up all the realizations of the random walk:

$$\xi_a(\boldsymbol{x}) = \frac{1}{N_{\rm real}} \sum_{J=1}^{N_{\rm real}} \boldsymbol{\xi}_0[b_J^{\boldsymbol{x}}(a)]\, {\rm e}^{S_J^{\boldsymbol{x}}(a)}. \tag{25}$$

(v) Having found the solution at the time corresponding to $a$, we iterate from step (ii), until the final time is reached.

Analogously to the free-diffusion case, we give a graphical representation of the solution corresponding to the above algorithm (Fig. 1b). Again a random walk starting from $\boldsymbol{x}$ at $a = a_0$ is drawn, and the initial field $\xi_0$ is computed at the projected points corresponding to the Eulerian position reached by the random walks $\boldsymbol{b}_a$. However, in this case, for computing the field $\xi_a$ at time $a$ the function $\xi_a[\boldsymbol{b}(a' < a)]$ has to be computed at all previous times (see point iii), since they constitute the argument of the potential $V_1$ entering equation (21).

A very important point emerging from the above solution of equation (14) is that the value of the field $\xi(\boldsymbol{x}, a)$ at a given coordinate $\boldsymbol{x}$ does indeed depend on the value of the field at other coordinates. In fact, for computing the field at the point $\boldsymbol{x}$, the functions $\xi_{a'<a}$ entering the potential $V_1$, must be computed at all points $\boldsymbol{b}(a')$. This is at variance with the case of simple diffusion, where all is needed to compute the solution is the *initial* field $\xi_0$ and the *final* localization of the random walk $\boldsymbol{b}(a)$. Of course, such property enters *only* when the 'interaction' potential $V_1$ is set in. This shows that even the first-order term $V_1$ in equation (14) introduces the typical effects of the non-linear dynamics, i.e., the influence on the velocity field of (a) the changes of it occurred at all previous times, and of (b) the value taken by the field in all other Eulerian points.

Thus we expect that the resulting dynamics 'feels', at some level, the changes of the fields in the course of evolution, a feature that is completely missing in the AA, as discussed above.

## 5 RESULTS AND COMPARISON WITH *N*-BODY SIMULATIONS

To test the above method for solving equation (14) and whether restricting to the term $V_1$ in equation (14) gives an accurate description of the non-linear dynamics, we compare the outcomes of the proposed description with those of an $N$-body cosmological simulation. Although a complete, systematic comparison between the $N$-body and the semi-analytic descriptions – including, e.g., different cosmological/cosmogonical initial conditions – is out of the scope of this paper, we will compare the density distribution and some statistical indicators which are believed to describe to some extent the matter field in the non-linear regime, for a given cosmological initial condition.

To perform the simulation, we adopt an adaptive P3M $N$-body code (see Hockney & Eastwood 1981 and Couchman 1991 for a detailed description) for self-gravitating, collisionless dark matter. In particular, we use the public version of the Couchman's adaptive P3M code (Couchman, Thomas & Pearce 1995) for the evolution of the dark matter, which was also used to generate the initial velocity field which is evolved both by the $N$-body and (according to our description) after equation (14).

To emulate the behaviour of the cosmological dark matter fluid, a distribution of $64^3$ particles is evolved in a comoving simulation box with periodic boundary conditions; the initial positions are assigned to be at the centre of the cells of a $64^3$ cubic grid. The initial displacement (velocity) is given by $\boldsymbol{u}_0 = \nabla\psi_0 \dot{a}\,{\rm d}a$ (we use a definition of the velocity potential rescaled to the Hubble expansion; see Section 2). The initial velocity potential is derived under the approximation (valid in the early, linear regime) $\psi_0 = -\phi_0$, where the initial potential is a Gaussian random field with power spectrum $\mathcal{P}_\phi(k) = Ak^{n-4}T^2(k)$, as it is commonly taken for primordial cosmological perturbations. The transfer function $T(k)$ depends on the nature of the dark matter field; here we adopt the form appropriate for cold dark matter (Davis et al. 1985; for recent fitting forms see Eisenstein & Wu 1999 and reference therein). The spectrum is normalized to the data from *COBE* (Stompor, Gorsky & Banday 1995; Bunn & White 1997). We assume a flat cosmology with matter density parameter $\Omega = 1$ and Hubble constant $h = 0.5$ (in units of $100\,{\rm km\,s^{-1}\,Mpc^{-1}}$). The physical length of the simulation cube is $L = 64\,h^{-1}\,{\rm Mpc}$; the gravitational force was softened at small distance, and the adopted softening parameter corresponds to 0.2 in mesh units.

To evolve an initial spatial distribution of particles according to our description, equation (14) is solved for both the case of free-diffusion (corresponding to the AA), and for a source term given by $V_1$ defined by equation (14b) (the EA model). At each cosmic time, the solution of equation (14) for the transformed velocity field $\xi(\boldsymbol{x})$ is found by generating, for each $\boldsymbol{x}$, a number $N_{\rm real}$ of random walks $\boldsymbol{b}(a)$ through a Monte Carlo procedure, as described in detail in Section 4.3. After transforming back to the velocity potential $\psi = -2\nu \ln \xi$, the position $\boldsymbol{x}(a)$ of each particle is then updated at each time-step to the new position $\boldsymbol{x}(a + {\rm d}a) = \boldsymbol{x}(a) + \boldsymbol{u}_a(\boldsymbol{x})\,{\rm d}a = \boldsymbol{x}(a) + \nabla\psi_a(\boldsymbol{x})\dot{a}\,{\rm d}a$.

The space grid used for the Monte Carlo solution described in Section 4.3 is taken to coincide with the $64^3$ simulation box. As for the number of realizations of the random walks, it has been checked that convergence in the solutions is obtained already for $N_{\rm real} \geq 10^2$ (the latter value requiring $\approx$100 Mbyte of computer memory; of course, the larger the value of $N_{\rm real}$, the larger is the requested memory and the slower is the numerical implementation); performing a test for the free-diffusion case with Gaussian initial conditions, a value $N_{\rm real} = 10^2$ yields errors $\delta\xi/\xi_{\rm exact} \leq 10^{-3}$ when the numerical solution is compared to the exact one $\xi_{\rm exact}$, whose analytical form is known in this case; the results shown below are obtained for $N_{\rm real} = 100$. To numerically implement our description, we adopt a finite value of the viscosity. Since we adopt the adimensional expansion factor $a$ as the 'time' variable in the equations for the velocity field (see equation 1, and equations 9 and following) the viscosity has the dimension of Length$^2$; we adopt the value $\nu = 10^{-1}\,{\rm pixel}^2$ (the pixel corresponding to the mesh size), which ensures convergence in the sense that results with smaller values of $\nu$ are indistinguishable;

a discussion on the physical effects of adopting different values of $\nu$ in the AA is given in Weinberg & Gunn (1990a).

While in the case of the AA and EA the velocity potential $\psi_a$ is obtained from equation (14), we recall that for *N*-body simulations the same displacement is obtained from the particle density field after solving the Poisson equation on the grid and integrating the resulting acceleration field. Thus, in such simulations, once the particles are moved, the resulting density field has to be recomputed to allow for solving the Poisson equation at the next time-step. Such a procedure, as well as double Fourier-transforms required to compute the solution of the Poisson equation, is not needed in the semi-analytic approaches, like the AA or EA, making them usually much faster than the simulations. In our case, the main source of time-consumption in the numerical implementation is due to the large number $N_{\rm real}$ of Monte Carlo realizations of the random walk needed to obtain reliable averages in equation (21).

The simulations are started at an initial time corresponding to an expansion factor $a_0 = 1/16$ (normalized as to yield $a = 1$ at the present time). The resulting particle distribution at the final time $a = 1$ is shown in Fig. 2 for the *N*-body simulation (left panel), the AA (middle panel) and the EA (right panel) for a slice 4 Mpc thick. The set of parameters adopted for the *N*-body simulation and for the AA and EA implementation are recalled and summarized in the caption.

Compared to the simulation, the AA reproduces well the general texture of LSS, but the small-scale features are underproduced. In particular, while in the simulations extended structures appear fragmented into dense knots, in the AA they appear more as a continuous filament. This is because the effects of the changes of the field in the course of evolution (typical of the non-linear regime) are neglected in the AA; since small scales are those which are evolved more deeply into the non-linear regime, it is natural that the AA does not reproduces them in detail. On the other hand, the EA seems to provide a more satisfactory description of the density field down to small scales; knotty, small-scale features are remarkably similar to those arising from the simulation, as is apparent, e.g., from the structures just above and below the large void at the centre of the picture. Most of the structures appearing in the simulations are reproduced by EA which seems to reproduce quite well the various degrees of clumpiness.

Thus the EA seems to improve the adhesion approach in that it provides a better description the fragmentation of filaments in correspondence of the denser knots. Such interpretation is confirmed by the more quantitative analysis performed in Fig. 3, where it is shown the deviation of the density field computed in the AA (top panel) or in the EA (bottom panel) from that resulting from the *N*-body simulation.

The comparison is performed on the same slice shown in Fig. 2, but limited to the region surrounding the big central void to provide a more clear graphical rendition. Note that the deviations of the AA density field are considerably larger than those occurring in the EA. More importantly, while the map of the deviation in the EA shows no obvious spatial structure, the deviation map of the AA clearly shows larger deviations correlated with the location of the filaments; even the perimeter of the large central void of Fig. 2 can be recognized in the AA map (top panel) of Fig. 3. Again this is related to the lack of fragmentation of filamentary structures typical of the AA.

The above differences, of course, can be traced back to the modification of the AA velocity field induced by the 'potential' term $V_1$ in equation (14). To show this in detail, the velocity field in the AA (top panel) and the EA (bottom panel) is represented in Fig. 4. For better readability, the plot refers to a further blow-up of the slice in Fig. 2, namely the region just above the big void (coordinates are specified in the caption), where the AA and EA yield clearly different degree of clumpiness. Inspection of Fig. 4 shows that the main, large-scale streams are indeed very similar; however, in the EA a modulation of such large-scale flows appears, resulting into a break-up of the coherent motions (defining the filamentary regions) into more structured velocity configurations, which are responsible for the formation of knots along the filaments.

The above consideration about the mass distribution in the different schemes can be tested more quantitatively through the computation of some basic statistical indicators. In particular, the correlation function $\Xi(r)$ and the rms density $\langle\delta_N^2\rangle^{1/2}$ are computed as a function of the scale $r$, where the latter is obtained by counting the density of particles in cells with radius $r$, and averaging over the simulation volume. The results are shown in Fig. 5 for redshifts $z = 1$ and $z = 0$. Note that, while at large scales

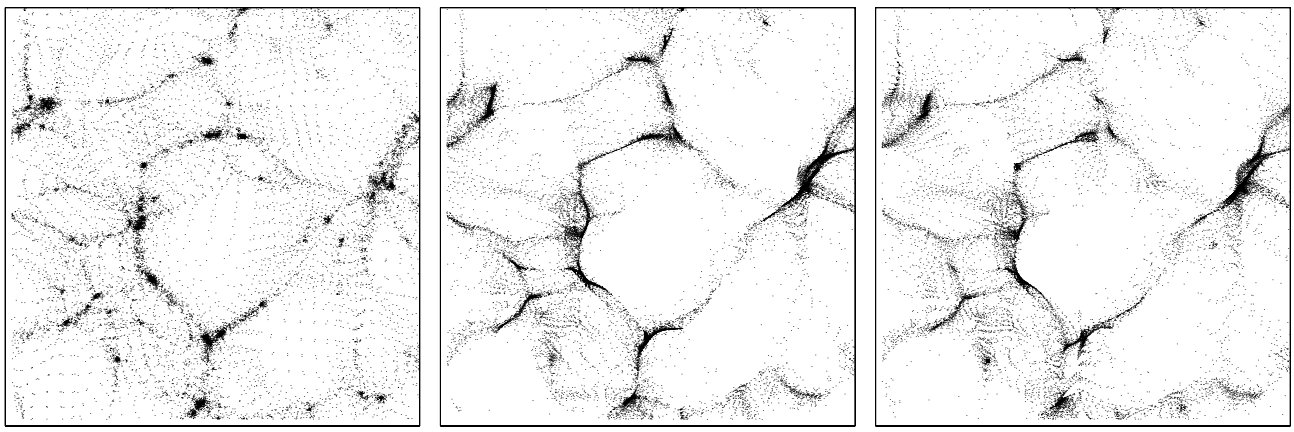

**Figure 2.** Slices through the particle distribution at redshift $z = 0$ from the *N*-body simulation (left panel), the adhesion approximation (middle panel) and the extended adhesion model (right panel) proposed in this paper. Each slice is 4 pixels thick, while the simulation box occupies a $64^3$ grid. Initial conditions from a *COBE*-normalized CDM power spectrum in an $\Omega = 1$ universe with Hubble constant $h = 0.5$. The parameters used for the *N*-body and for the Monte Carlo implementation of the AA and EA are the following: physical length of the simulation cube $L = 64\,h^{-1}$ Mpc; initial expansion factor $a_0 = 1/16$ (assuming that $a = 1$ at the present time); the Plummer softening parameter adopted in the *N*-body simulation is 0.2; the number of Monte Carlo realizations used to obtain the velocity field for the AA and EA is $N_{\rm real} = 10^2$; the artificial viscosity is $\nu = 10^{-1}$ (mesh units)$^2$.

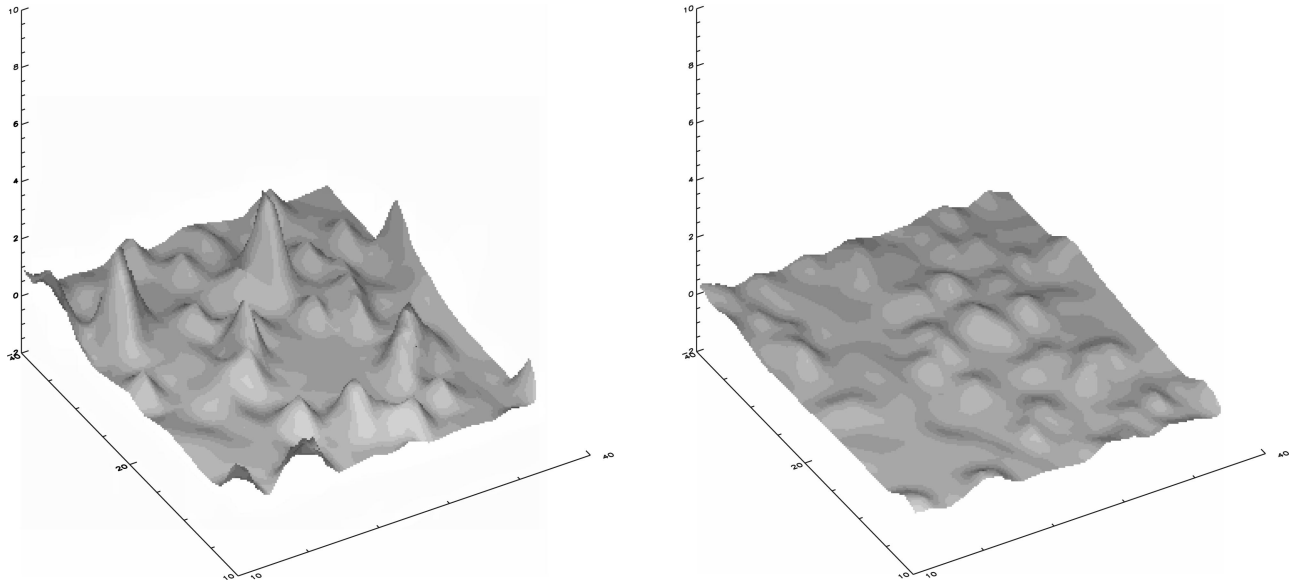

**Figure 3.** The overdensity $(N - N_{N-\mathrm{body}})/N_{N-\mathrm{body}}$ of the particle density $N$ resulting from the AA (left-hand panel) and from the EA (right-hand panel) with respect to the particle density from the $N$-body simulation $N_{N\text{-body}}$ is plotted as a function of the $x-y$ coordinates, for the same $z$-plane as for Fig. 2. The $x-y$ region of the maps is a blow-up of the central region of the slice in Fig. 2, smoothed with a radius of 2 pixels.

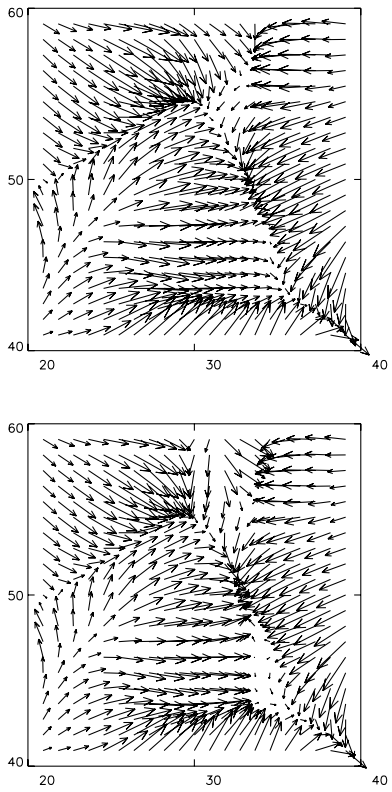

**Figure 4.** The Eulerian velocity field from the AA (top panel) and from the EA (bottom panel) is shown for the region ($20 < x < 40$, $40 < y < 60$ in units of the pixel size) just above the void in Fig. 2. The length of the arrows is proportional to the modulus of the velocity.

the AA gives a fair description of the density field at $r \gtrsim 5$ Mpc, at small scales it underestimates both the correlation function and the average density, as already obtained by Weinberg & Gunn (1990a). The same statistical properties seem to be well reproduced by EA, as it is shown by the agreement with the $N$-body results in Fig. 5, which is preserved down to the resolution limit of the simulations. Again, this is due to the fact that structures in the AA arise directly from features in the initial conditions, while the EA, to some extent, captures the effect of the changes that the matter field undergoes in the course of evolution.

## 6 CONCLUSIONS

A description of the dynamics of a collisionless, self-gravitating fluid has been developed and applied to follow the development of large-scale structures in the Universe. Such description takes on one of the assumptions of the adhesion approximation (AA) model, i.e., the introduction of an artificial viscosity in the Euler equation, but extends it beyond the approximation which make it strictly valid only in the linear regime, namely the assumption of equality between the velocity and the gravitational potential, $\psi = -\phi$. The key points characterizing the proposed approach (extended adhesion, EA) can be summarized as follows.

(1) The dynamics emerging from such a novel description is determined by a diffusion-like equation for the transformed velocity potential $\xi = \exp(-\psi/2\nu)$. Such an equation includes a source term $V(\xi)$ (or an 'interaction' term in the action, if the diffusion equation is considered like a Shrödinger equation in Euclidean time) which grows from zero (the limit corresponding to the AA) with increasing time; this in fact describes the onset of non-linear evolution of the velocity potential. The AA is then recovered, in path-integral language, as a free-particle theory.

(2) When the 'potential' $V(\xi)$ is expanded in powers of the small artificial viscosity $\nu$, the term corresponding to the lowest order can be expressed in a fully Eulerian form. In this case it is possible to compute a solution for $\xi$ based on the realization of random walks in the Eulerian space. The solution at the time $a$ and at the point $\boldsymbol{x}$ is related to a proper sum over the fields computed at the preceding times at the Eulerian coordinates reached by a Gaussian random walk starting from $\boldsymbol{x}$ at the initial time.

(3) Such a solution of the diffusion equation explicitly shows that the source term introduced in the proposed extension of the AA affects the dynamics in two key respects: (i) the velocity

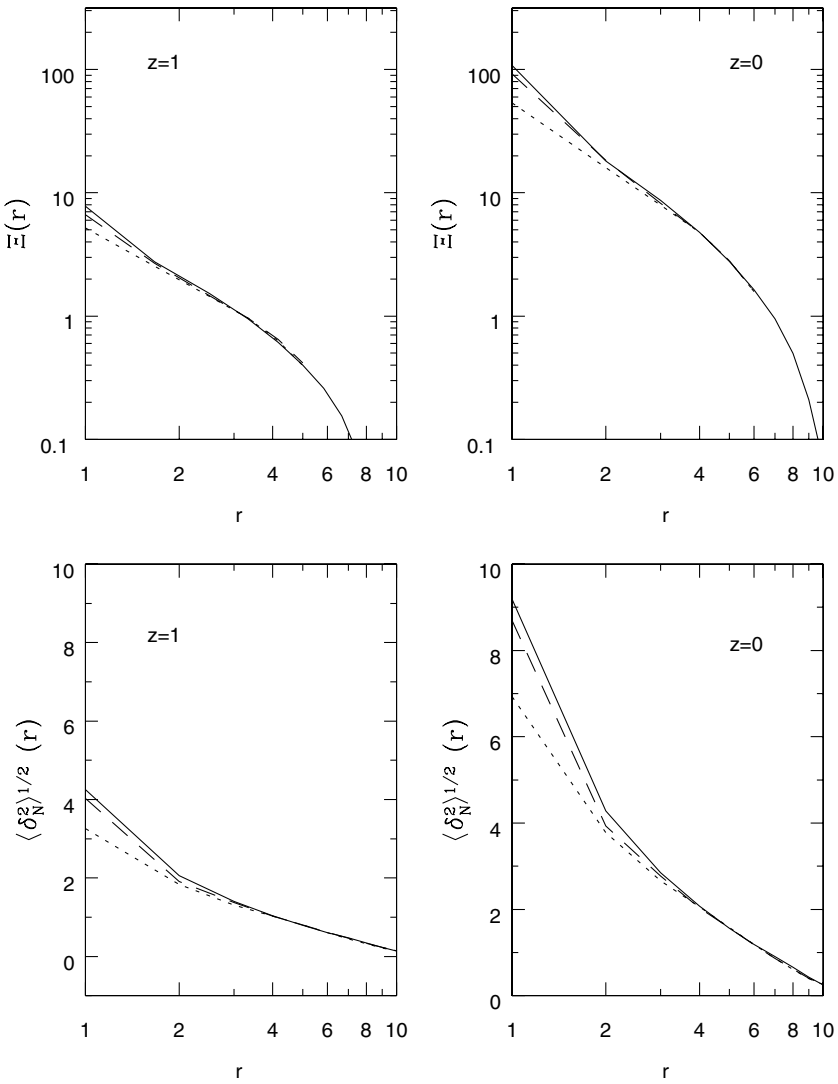


**Figure 5.** The two-point correlation function is shown in the top panels for the *N*-body simulations (solid line), the EA (dashed line) and the AA (dotted line). The bottom panels show the rms fluctuations of the density smoothed with a Gaussian of radius *r*. The latter is expressed in pixels units; different lines correspond to the models as above. The left-hand column refers to $z = 1$, while the right-hand column refers to $z = 0$.

potential $\psi$ at a given time is no longer determined by its initial form, but depends on the values taken at all previous times; (ii) the value taken by $\psi$ at a given point depends on the value taken at the other points. Both these features are characteristic of the non-linear dynamical regime, when the density and fluctuations cease to evolve independently and 'feel' the effect of the whole mass distribution.

Thus the proposed extension of the adhesion approximation is expected to provide a better description of the regions which underwent a deeper non-linear evolution. To test such expectation, the solution for the velocity field in the EA approach has been used to compute the time evolution of a cosmological dark matter field, and the results have been tested against *N*-body simulations.

When one restricts to consider a null source term $V(\xi) = 0$, the AA with finite viscosity is recovered. In this case our results and comparison with the *N*-body simulations yield results similar to those in Weinberg & Gunn (1990a), as is shown qualitatively by the particle spatial distribution (Fig. 2), and quantitatively by the correlation function and mean overdensity plots. However, the random walk approach adopted here yields shorter computational time than the Gaussian convolution method adopted by the above authors, resulting in a gain over the simulation by a factor of 2–3.

When the 'interaction' term $V_1$ is set in, the evolution of the velocity field in the EA approach is successful in reproducing most of the features emerging from the *N*-body simulations, including the fragmentation of large-scale structures into dense lumps. The correlation function an the mean overdensity as a function of scale resulting from our EA model agrees remarkably well with those from the *N*-body, even at small scales (see Fig. 5). At larger scales and for underdense regions, our extension of the Zel'dovich Ansatz $\psi = -\psi$ leaves invariant the satisfying agreement of the Zel'dovich and adhesion approximations with the outcomes of the simulations; this is at variance with other semi-analytic approaches to LSS (like the Lagrangian perturbation theory to second order Bouchet et al. 1995).

The above results indicate that the lowest order term $V_1$ in the equation for the velocity potential is effective in capturing some relevant features of the non-linear evolution of the velocity field. The physical meaning of such a term, as compared with the higher order one $V_2$ entering equation (14), is straightforward. Inspection of equation (14b) and of the Hopf–Cole transformation $\xi =$

$\exp(-\psi/2\nu)$ shows that such a term corresponds to considering the effect of the *time average* of the velocity potential in the course of evolution. Thus the solutions presented here correspond in a sense to 'mean field' solutions. It is not surprising, then, that these constitute the lowest order correction to the 'free-particle' behaviour, corresponding to the AA. The consideration of higher order terms in $V(\xi)$ would then correspond to a consideration of the detailed effect of each single particle on the evolution of the Eulerian velocity potential. This effect, of course, is related to the detailed history of each particle, and correspondingly it is expressed by non-local terms which involve integrals over the particle trajectory, like those in the term $V_2$ entering equation (14).

## 7 DISCUSSION

As recalled above, the dynamics described by the EA through the time-evolving velocity potential derived from equations (14a) and (14b) allows us to improve the description of the high-density regions, more deeply evolved in the non-linear regime. This improvement allows us (i) to extend the insight on the physics of LSS to include the evolution of higher density regions, and (ii) to extend the cosmological applications of the ZA and EA to a larger density range, including overdensities up to (at least) $\delta \sim 10$ (see Fig. 5) where the EA (at variance with ZA and AA) still provides a satisfactory description. We shall now discuss the above two points in turn.

Previous works based on *N*-body simulations (Melott, Weinberg & Gott 1988) and on implementations of the AA (Weinberg & Gunn 1990a) suggested that on sufficiently large scales the process of non-linear gravitational evolution may be viewed as a smoothing process on the initial density field; indeed, the results for the AA (Weinberg & Gunn 1990a) showed that the density field resulting at a given cosmic time is well approximated by the initial density field smoothed over a scale corresponding to $\approx\overline{\Delta x}/3$, where $\overline{\Delta x}$ is the average particle displacement at that time (i.e., the average comoving distance that a particle has moved from its initial position). The AA allows us to pin down the origin of such a behaviour; indeed, for large scales where the AA is a satisfactory approximation, the *diffusion* term in the Burgers equation for the velocity field (or equivalently in equation 1 for the velocity potential) has the effect that the velocity field at a point incorporates the contributions from the surrounding patch of initial conditions. This is explicitly shown by the corresponding form of the velocity potential (equations 3 and 4) and by the random walk solution illustrated in Fig. 1; as noted by Weinberg & Gunn (1990a), the non-linear Hopf–Cole transformation $\psi \rightarrow \xi$ in the solution of the Bernoulli equation (1) amplifies gradients so that the diffusive smoothing has the greater impact where it is most needed. The latter point is shared by the EA; however, the graphical illustration (Fig. 1) of the EA solution for the velocity field shows that, for sufficiently large times at the onset of the term $V_1$, a second process overlaps the diffusive smoothing in determining the evolution of LSS; in fact, the velocity field at a point is now influenced by the value of the field at times closer to the present, as shown in detail in Fig. 1. Thus, regions with larger overdensities (corresponding to larger velocities in the surroundings) acquire a larger and larger role in driving the evolution of $\psi$, and this has the effect of enhancing the inhomogeneities in the density field. This is apparent also from the path-integral solution in equation (20), which shows that the random diffusion term [the 'kinetic' part of the action $\propto(\mathrm{d}\boldsymbol{b}/\mathrm{d}s)^2$ which corresponds to the 'smoothing' mode] is now complemented by the potential term $V(\xi)$; of all the paths that contribute to the integral, those passing through maxima of $V(\xi)$ (at *evolved* times) make the dominant contribution to the integral. Thus the potential term in equation (20) acts like a 'selection' term (in contrast with the 'smoothing' term driving the whole dynamics in the AA), which progressively weights the more non-linear regions in determining the evolution of $\xi$. It is this latter effect which drives the fragmentation of filaments into several knots (see Figs 2–4) observed at late times in *N*-body simulation and missing from the AA dynamics. Inspection of Fig. 5 shows that such a second mode in the LSS evolution begins to efficiently overlap to the diffusive smoothing already at $z \sim 1$. Thus the non-linear gravitational evolution can be viewed as smoothing process of the initial conditions for $\delta < 5$, as suggested by previous works on the AA; for larger overdensities at $z < 1$ the velocity gradient induced by small-scale overdensities overlaps to the smoothing mode so that particles flow along the filaments to enhance small-scale overdensities, partially breaking the extended structures into dense knots. A finer description of such process includes the effect of each particle trajectory in the modification of the velocity field, and corresponds to the term $V_2$ in equation (14).

As to the investigation of cosmological problems, the EA can be used to complement *N*-body simulations in several ways: first, the shorter computational time taken by the EA to run allows a more extensive exploration of the parameter space in many astrophysical problems; second, the EA can be used in the development or testing phase of investigation techniques which require a large number of simulations; third, it can be used to estimate the probability for a given configuration (both in density and in velocity) to occur, a problem which may also require running a large number of simulations. It must be noticed that the above advantages are shared with other approximations like the ZA and the AA; however, the EA allows to describe a wider range of overdensities (see, e.g., Fig. 5), thus extending the fields of investigation and allowing us to address additional problems. A first example is constituted by the study of Ly$\alpha$ regions and, in general, by the comparison of theoretical predictions with the observations concerning the intergalactic medium. Indeed, several authors have used the ZA (with an appropriate smoothing on initial conditions) to study the distribution of Ly$\alpha$ column densities (Hui, Gnedin & Zhang 1997; Gnedin & Hui 1998); the density and velocity field derived from ZA were related to the gas density, temperature and composition by an independently derived equation of state. The resulting distribution of Ly$\alpha$ column density can be compared with observations, and a large variety of parameters (concerning the cosmology, the equation of state of the gas, the reionization epoch and the ionizing radiation) can explored through the use of the fast ZA algorithm. However, such an approach could be applied only for density contrast $\delta < 5$ (corresponding to column densities $< 10^{14.5}\,\mathrm{cm}^{-2}$) due to the break down of the ZA (and also of the AA, as shown by Fig. 5) at higher density contrast. In this context, the EA could extend the range of such investigations to larger density contrast and hence to larger column densities. In this context, such investigations could be further extended to include (at least partially) baryons at temperatures $\sim 10^5$–$10^6$ K residing in higher density contrast $\delta \gtrsim 10$, which could constitute a relevant (if not major) fraction of all existing baryons (see, e.g., Cen & Ostriker 1999). While a full treatment of them requires full hydrodynamical simulations including shock-heating, preliminary studies and parameter exploration concerning the statistics of column densities of such gas could be performed through the EA. Once a smaller set of plausible models is identified with this technique, full hydrodynamical simulations can be run. Further examples of

cosmological studies through the EA can be constituted by the computation of the density distribution produced in the mildly non-linear regime extending to density $\delta \sim 10$ in a variety of cosmological conditions; this enters many analytical or semi-analytical computations concerning the thermal and chemical state of the intergalactic medium (which are also being included in semi-analytic models of galaxy formations; see Benson et al. 2001). Additional applications concern the extension to larger overdensities of a reliable velocity–density relation (widely investigated with the use of the ZA up to densities $\delta \lesssim 4$; see Nusser et al. 1991, and also Weinberg & Gunn 1990b), particularly used for the analysis of large-scale flows and for the inverse problem of deriving the velocity field corresponding to observed galaxy distribution.

Besides complementing the *N*-body simulations in evolving numerically a dark matter field, the compact, analytical form (equation 14) for the evolution of the velocity field constitutes a promising way to study directly and analytically relevant scaling properties for the collisionless fluid. In particular, it is known that the solution of equations similar to (14) with a random source term $V$ show interesting fractal (Brax 1992) and intermittency (Gärtner & Molchanov 1992) properties. Indeed, an approach involving a diffusion equation with a source term for the velocity field has been used by Jones (1999) to relate the *baryonic* velocity field (the one following the diffusion equation in such model) to the dark matter potential (the source term) which, in this approach, is given as an input. The intermittency and fractal properties of the baryonic velocity field in this model (which give rise to nice scaling properties of the resulting galaxy distribution) are probably features which are shared by the velocity field in our model. While the investigation of such issues is more complicated in the EA than in the AA or ZA due to the more complex form of the velocity potential, it is nevertheless interesting to study the effects of the non-linear source term introduced by the EA in the Burgers equation on the fractal and intermittency properties of the resulting velocity field, since this would provide useful analytical tools to characterize the growth of LSS in a more evolved non-linear stage than that probed by previous approximations. The investigation of such a point will be the subject of a later paper.

## ACKNOWLEDGMENTS

I thank S. Borgani, E. Giallongo and S. Matarrese for helpful discussions, and the referee for his constructive comments.

## REFERENCES

Bagla J. S., Padmanabhan T., 1994, MNRAS, 266, 227
Benson A. J., Lacey C. G., Baugh C. M., Cole S., Frenk C. S., 2001, preprint (astro-ph/0108218)
Bertschinger E., 1998, ARA&A, 36, 599
Brainerd T. G., Scherrer R. J., Villumsen J. V., 1993, ApJ, 418, 570
Bouchet F. R., Colombi S., Hivon E., Juskievich R., 1995, A&A, 296, 575
Buchert T., Dominguez A., 1998, A&A, 335, 395
Buchert T., Ehlers J., 1993, MNRAS, 264, 375
Brax P., 1992, Phys. Lett., A165, 335
Bunn E. F., White M., 1997, ApJ, 480, 6
Cen R., Ostriker J. P., 1999, ApJ, 519, L109
Coles P., Chiang L., 2000, Nat, 406, 376
Couchman H. M. P., 1991, ApJ, 368, 23
Couchman H. M. P., Thomas P. A., Pearce F. R., 1995, ApJ, 452, 797
Davis M., Efstathiou G., Frenk C. S., White S. D. M., 1985, ApJ, 292, 371
de Lapparent V., Geller M. J., Huchra J. P., 1986, ApJ, 301, L1
Eisenstein D. J., Wu W., 1999, ApJ, 511, 5
Feynman R. P., Hibbs A. R., 1965, Quantum Mechanics and Path Integrals. McGraw Hill, New York
Gärtner J., Molchanov S. A., 1991, Commun. Math. Phys., 132, 613
Gnedin N. Y., Hui L., 1998, MNRAS, 296, 44
Gurbatov S. N., Saichev A. I., 1984, Isv. VUZ, Radiofizica, 27
Gurbatov S. N., Saichev A. I., Shandarin S., 1985, Sov. Phys. Dokl., 30, 921
Gurbatov S. N., Saichev A. I., Shandarin S., 1989, MNRAS, 236, 385
Hockney R. W., Eastwood J. W., 1981, Computer Simulations Using Particles. McGraw-Hill, New York
Hui L., Gnedin N. Y., Zhang Y., 1997, ApJ, 486, 599
Jones B. T., 1999, MNRAS, 307, 376
Kofman L., 1991, in Sato K., ed., Proc. IUAP Conference on Nucleosynthesis in the Universe. Kluwer, Dordrecht, p. 495
Kofman L., Pogsyan D., Shandarin S., Melott A., 1992, ApJ, 393, 437
Maddox S. J., Sutherland W. J., Efstathiou G., Loveday J., 1990, MNRAS, 243, 692
Matarrese S., Lucchin F., Moscardini L., Saez D., 1992, MNRAS, 259, 437
Melott A. L., Einasto J., Saar E., Suisalu I., Klypin A. A., Shandarin S. F., 1983, Phys. Rev. Lett., 51, 935
Melott A. L., Weinberg D. H., Gott J. R., 1988, ApJ, 328, 50
Melott A. L., Shandarin S. F., Weinberg D. H., 1994, ApJ, 428, 28
Melott A. L., Buchert T., Weiss A. G., 1995, A&A, 294, 345
Moutarde F., Alimi J., Bouchet F. R., Pellat R., Ramani A., 1991, ApJ, 382, 377
Munshi D., Starobinsky A. A., 1994, ApJ, 428, 433
Munshi D., Sahni V., Starobinsky A. A., 1994, ApJ, 436, 517
Nusser A., Dekel A., 1990, ApJ, 362, 14
Nusser A., Dekel A., Bertschinger E., Blumenthal G. R., 1991, ApJ, 379, 6
Peebles P. J. E., 1993, Principles of Physical Cosmology. Princeton Univ. Press, Princeton
Sahni V., Coles P., 1995, Phys. Rep., 262, 1
Sathyaprakash B. S., Sahni V., Munshi D., Pogosyan D., Melott A. L., 1995, MNRAS, 275, 463
Saunders W. et al., 1991, Nat, 349, 32
Shandarin S. F., Zel'dovich Ya. B., 1989, Rev. Mod. Phys., 61, 185
Shectman S. A., Landy S. D., Oemler A., Tucker D. L., Lin H., Kirshner R. P., Schechter P. L., 1996, ApJ, 470, 172
Stompor R., Gorsky K. M., Banday A. J., 1995, MNRAS, 277, 1225
Vergassola M., Dubrulle B., Frish U., Noullez A., 1994, A&A, 289, 325
Vogeley M. S., Park C., Geller M. J., Huchra J. P., 1992, ApJ, 391, L5
Weinberg D. H., Gunn J. E., 1990a, MNRAS, 247, 260
Weinberg D. H., Gunn J. E., 1990b, ApJ, 325, L25

## APPENDIX A

The quantity $Q_a = \int_{\mathcal{C}_a(x)} \Delta \ln \xi \, \mathrm{d}a'$ evolves according to the following relation

$$Q_{a+\mathrm{d}a}(\boldsymbol{x}) = Q_a(\boldsymbol{z}) + \Delta \ln \xi(\boldsymbol{z}) \, \mathrm{d}a, \tag{A1}$$

where $\boldsymbol{z}$ is the particle position at the previous time in the trajectory $\mathcal{C}(x)$, so that $\boldsymbol{z} = \boldsymbol{x} - \boldsymbol{u}_a(\boldsymbol{z}) \, \mathrm{d}a$. For small time increments $\mathrm{d}a$, the velocity in $\boldsymbol{z}$ is given by

$$\boldsymbol{u}_a(\boldsymbol{z}) = \boldsymbol{u}_a(\boldsymbol{x})[1 - \nabla \cdot \boldsymbol{u}_a(\boldsymbol{x}) \, \mathrm{d}a]. \tag{A2}$$

Substituting for $\boldsymbol{z}$ and for $\boldsymbol{u}_a(\boldsymbol{z})$ into equation (A1), one obtains

$$Q_{a+\mathrm{d}a}(\boldsymbol{x}) = Q_a(\boldsymbol{x}) - [\nabla Q \cdot \boldsymbol{u}_a](\boldsymbol{x}) \, \mathrm{d}a + \Delta \ln \xi(\boldsymbol{x}) \, \mathrm{d}a + O(\mathrm{d}a^2), \tag{A3}$$

from which, after substituting $\boldsymbol{u} = \nabla(-2\nu \ln \xi)$ (by definition of $\xi$), equation (12) follows.

As for equation (13), we note that

$$\boldsymbol{x} = \boldsymbol{q} - 2\nu \int_{a_0}^{a} \nabla \ln \xi[\boldsymbol{x}(\boldsymbol{q}, a')] \, \mathrm{d}a' \tag{A4}$$

From this it follows that

$$\Delta\ln\xi[\boldsymbol{x}(\boldsymbol{q},a+\mathrm{d}a)] = \Delta\ln\xi\Big\{\boldsymbol{q} - 2\nu\int_{a_0}^{a}\nabla\ln\xi[\boldsymbol{x}(\boldsymbol{q},a')]\,\mathrm{d}a' - 2\nu\nabla\ln\xi[\boldsymbol{x}(\boldsymbol{q},a)]\,\mathrm{d}a\Big\}. \tag{A5}$$

For small displacements $-2\nu\nabla\ln\xi[\boldsymbol{x}(\boldsymbol{q},a)]\,\mathrm{d}a$ along the particle trajectory, the expansion of the argument of the right-hand side yields

$$\Delta\ln\xi[\boldsymbol{x}(\boldsymbol{q},a+\mathrm{d}a)] = \Delta\ln\xi[\boldsymbol{x}(\boldsymbol{q},a)] - 2\nu[\nabla(\Delta\ln\xi)\cdot\nabla\ln\xi][\boldsymbol{x}(\boldsymbol{q},a)]\,\mathrm{d}a, \tag{A6}$$

whose iteration leads to equation (13).

This paper has been typeset from a TEX/LATEX file prepared by the author.